Influence of annealing on the photodeposition of silver on periodically poled lithium niobate

N. Craig Carville,[1,2] Sabine M. Neumayer,[1,2] Michele Manzo,[3] Mohammad-Amin Baghban,[3] Ilia N. Ivanov,[4] Katia Gallo,[3] and Brian J. Rodriguez[1,2,a)]
[1]*School of Physics, University College Dublin, Belfield, Dublin 4, Ireland*
[2]*Conway Institute of Biomolecular and Biomedical Research, University College Dublin, Belfield, Dublin 4, Ireland*
[3]*Department of Applied Physics, KTH - Royal Institute of Technology, Roslagstullbacken 21, 106 91 Stockholm, Sweden*
[4]*Center for Nanophase Materials Sciences, Oak Ridge National Laboratory, Oak Ridge, Tennessee 37831, USA*

(Received 5 November 2015; accepted 18 January 2016; published online 3 February 2016)

The preferential deposition of metal nanoparticles onto periodically poled lithium niobate surfaces, whereby photogenerated electrons accumulate in accordance with local electric fields and reduce metal ions from solution, is known to depend on the intensity and wavelength of the illumination and the concentration of the solution used. Here, it is shown that for identical deposition conditions (wavelength, intensity, concentration), post-poling annealing for 10 h at 200 °C modifies the surface reactivity through the reorientation of internal defect fields. Whereas silver nanoparticles deposit preferentially on the $+z$ domains on unannealed crystals, the deposition occurs preferentially along 180° domain walls for annealed crystals. In neither case is the deposition selective; limited deposition occurs also on the unannealed $-z$ domain surface and on both annealed domain surfaces. The observed behavior is attributed to a relaxation of the poling-induced defect frustration mediated by Li^+ ion mobility during annealing, which affects the accumulation of electrons, thereby changing the surface reactivity. The evolution of the defect field with temperature is corroborated using Raman spectroscopy. © *2016 AIP Publishing LLC*. [http://dx.doi.org/10.1063/1.4940968]

I. INTRODUCTION

The reversible spontaneous polarization of ferroelectric materials makes them suitable for applications (e.g., biosensing[1,2]) based on local control of surface reactivity,[3,4] which depends strongly on the polarization-dependent surface electronic structure and charge screening.[3,5,6] Polarization-dependent surface reactivity has been exploited extensively for the photoreduction of metallic nanoparticles.[1–4,6–26] Typically, when aqueous $AgNO_3$ solution is placed on a ferroelectric surface illuminated with super bandgap light, photogenerated electrons accumulate at the positive domain surface due to downwards band bending, leading to the deposition of Ag particles on the positive domains via the reduction of Ag^+ to Ag^0.[8,9,11,12] LN has proven to be an exception to this rule, whereby the metal particles have been found to deposit in some cases along the domain wall and on positive and negative domains in others, depending on the experimental conditions.[14,15,22–26] Dunn and Tiwari have suggested that photoelectrically generated electrons can reduce the Ag^+ bound to the negative surfaces and that the differences between reported results on positive domains and domain walls can be attributed to the wavelength and power of irradiation used, i.e., high power illumination creates a high flux of photons, which leads to complete domain coverage, whereas nucleation occurs only at 180° domain boundaries under low power illumination conditions.[24] Similarly, Sun *et al*. have reported that the differences in deposition on periodically poled LN (PPLN) are due to the ratio between the photon flux and the ion flux, which can be controlled via the illumination intensity and concentration of Ag^+ ions, respectively.[25] The location of the preferential deposition may also depend on the crystal history (e.g., thermal) and crystal quality, information typically absent from the literature.

To investigate how thermal treatments can affect photodeposition, it is important to first understand the influence of poling on internal electric fields. PPLN crystals are fabricated by selectively reversing the polarization direction upon the application of an electric field greater than the coercive field of the crystal using a periodic mask,[27] which induces strain in the regions exposed to the electric field.[28] Congruent LN is Li deficient, leading to nonstoichiometric defect clusters comprising one Nb antisite (Nb_{Li}) and four Li vacancies (V_{Li}),[29] which possess a polarization and a corresponding defect field that aligns with the depolarization field during crystal growth.[30] As described by Gopalan *et al*., upon poling, the Nb_{Li} antisites show the same behavior as Li ions and move through the oxygen plane to the second thermodynamically stable position in the neighboring octahedron.[31] However, due to the low mobility of Li^+ at room temperature,[32] the positions of the V_{Li} remain the same, leaving the polar orientation of the defect cluster in the poled region in a frustrated state. There is, therefore, an asymmetry in the internal electric fields for oppositely poled domains, whereby the parallel depolarization and defect fields in the

a)Author to whom correspondence should be addressed. Electronic mail: brian.rodriguez@ucd.ie

as grown crystal become antiparallel in the poled domain after poling.[27–30,32–34] Annealing the crystal at temperatures >150 °C is known to mobilize Li^+ ions, allowing the internal defect field to realign parallel to the depolarization field, thus alleviating the defect frustration.[35,36] Annealing therefore provides a mechanism to modify the internal defect field and by extension, the photodeposition. Here, the role of annealing on the photochemistry of PPLN crystal surfaces is explored.

II. EXPERIMENTAL DETAILS

Standard photolithography was employed to fabricate 1D (34 μm period) and 2D (22.8 μm period) periodic openings in photoresist on the $-z$ sides of 0.5 mm thick, z-cut congruent LN crystal substrates (CasTech, Inc., China) and a bias applied via a conductive gel was used to switch the polarization of the crystals at the exposed surfaces, resulting in arrays of domains with opposite polarization.[37] The original $-z$ side of the 1D (or 2D) PPLN sample is further referred to as $-z$ 1D (or 2D) PPLN, whereas the corresponding initial +z side is called +z 1D (or 2D) PPLN. The samples were processed in duplicate, and one of each of the 1D and 2D samples was annealed post-poling for 10 h at 200 °C with a 1–3 °C/min ramp rate using a hot plate (HP1, Clifton, Ireland). The same rate was used to cool the sample to room temperature.

After patterning and annealing, the samples were cleaned for 20 min each in acetone, isopropanol, and milliQ water (Gradient A10, Millipore, 18.2 MΩ·cm) via sonication. 100 μl of 0.01 M concentration aqueous $AgNO_3$ was subsequently pipetted onto the surface, and the samples were illuminated for 5 min from a distance of 2 cm above the sample with a 254 nm light source (11SC-2, Spectroline, USA) with a specified power density of 2000 $\mu W/cm^2$ and corresponding photon energy greater than the reported bandgap of LN (3.9 eV (Ref. 38)). After illumination, the samples were rinsed with milliQ water for 1 min and dried using compressed nitrogen.

Amplitude modulation mode atomic force microscopy (AFM) (MFP-3D, Asylum Research, USA) was used to image the samples before and after the UV illumination with cantilevers having a typical resonant frequency of ~330 kHz and spring constant of ~42 N/m (PPP-NCH, Nanosensors, Switzerland). A contact mode voltage-modulated AFM technique, piezoresponse force microscopy (PFM),[39,40] was used to visualize the ferroelectric domains prior to UV exposure. Pt-coated Si probes (HQ:NSC15, MikroMasch, Germany) with a nominal resonant frequency of 325 kHz and a nominal spring constant of 40 N/m were used for PFM measurements. A 5 V AC voltage at 800 kHz (below contact resonance) was applied to the tip. This resulted in surface deformations due to the converse piezoelectric effect, which were detected at the modulation frequency via a lock-in amplifier (HF2LI, Zurich Instruments, Switzerland). The resulting signal was demodulated into amplitude and phase signals, which were used to determine the amplitude of the bias-induced piezoelectric deformation and the orientation of the spontaneous polarization, respectively. The PFM images were acquired simultaneously with topography. AFM topography images were first order plane-fit flattened, while PFM images were not flattened. Height differences are reported as the mean ± the standard deviation calculated from 10 line profiles.

Raman spectra from 100 to 1200 cm^{-1} were measured with a confocal Raman spectrometer (Renishaw 1000, UK) by focusing a laser ($\lambda = 532$ nm) on unannealed or annealed PPLN surfaces through a 100× or 50× objective, respectively. The signal was collected in $\bar{Z}(XX)Z$ backscattering geometry through the same objective. As poling was initiated at the initial $-z$ side, Raman maps were acquired at the original $+z$ side in order to preclude effects of fringe fields and the photolithographic mask. The maps were acquired with a 500 nm step in x- and y-directions and a 10 s integration time $+z$ 2D. The Raman spectrometer was calibrated using a 520.5 cm^{-1} characteristic Si line. All spectra were normalized with respect to the highest peak intensity and then fitted with a mixture of Lorentzian and Gaussian functions with a linear baseline correction. Peak fitting parameters included peak intensity, position, and full width at half height (FWHM) for each spectrum, from which image maps were constructed using interpolation of neighboring pixels.

III. RESULTS

The topography of the 1D PPLN surfaces before and after annealing has been imaged using AFM in order to determine if the surface roughness is influenced by annealing (Fig. 1). The topography of the unannealed $-z$ 1D PPLN sample is shown in Fig. 1(a), and a representative line profile is shown in Fig. 1(b). From the analysis of the 20 × 20 μm image (Fig. 1(a)), the surface roughness is determined to be 0.45 ± 0.09 nm root mean square (rms). The topography of the annealed surface ($-z$ side) is shown in Fig. 1(c), which has a roughness of 0.45 ± 0.03 nm rms. A representative line profile is shown in Fig. 1(d). The roughness analysis illustrates that annealing does not significantly change the surface

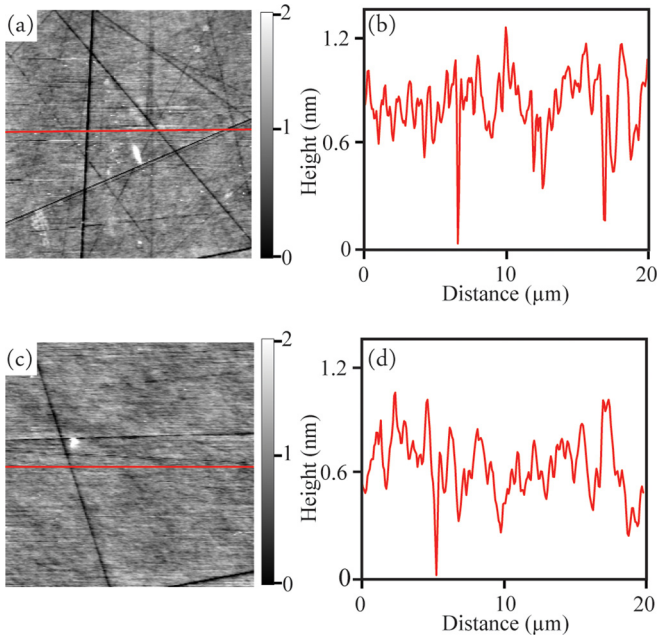

FIG. 1. (a) AFM topography image of an unannealed sample prior to photodeposition and (b) representative line profile. (c) AFM topography image of annealed sample prior to photodeposition and (d) representative line profile.

topography or roughness on either side of the 1D and 2D PPLN samples.

The PFM phase and amplitude images for the unannealed $-z$ 1D PPLN side that was of negative polarization before poling are provided in Figs. 2(a) and 2(c). Representative line profiles of PFM phase and amplitude are shown in Figs. 2(b) and 2(d). The positive and negative domains are separated by domain walls, which appear as dark lines in the PFM amplitude image (Fig. 2(c)). The periodic poling pattern is also evident in the PFM phase image (Fig. 2(a)) and the line profile (Fig. 2(b)), which show that adjacent domains oscillate ~180° out of phase from each other under the applied field. The inset images correspond to a region containing nanodomains, which can occur during poling, as previously reported by Shur *et al.*[41,42] PFM images of the initial $+z$ side and on both sides of the 2D PPLN samples (not shown) were qualitatively similar.

The topography of the unannealed $-z$ 1D PPLN crystal surface after deposition is illustrated in Figs. 3(a) and 3(c). The Ag deposition occurs on both the positive and negative domain surfaces, as illustrated by the line profiles (Figs. 3(b) and 3(d)). The rms roughness of the area corresponding to the negative domain is 0.98 ± 0.08 nm, while the roughness for the positive domain is 1.38 ± 0.13 nm, indicating that Ag has deposited in both regions. The average height difference between the positive and negative domains, determined from line profiles, is 2.84 ± 0.24 nm and corresponds to the differential thickness of the Ag deposition.

The results of photodeposition experiments performed under the same experimental conditions on the annealed 1D PPLN crystal are illustrated in Fig. 4. The Ag deposition is more pronounced at the 180° domain walls, in agreement with the previous reports.[14,25,26] The average relative height of the Ag nanowires, determined from line profiles, is

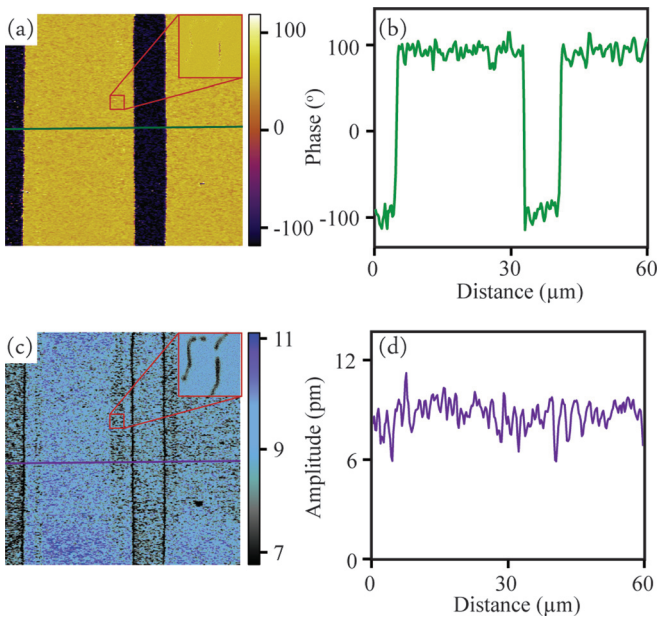

FIG. 2. (a) PFM amplitude image of unannealed sample prior to photodeposition and (b) representative line profile. (c) PFM phase image of unannealed sample prior to photodeposition and (d) representative line profile. Insets in (a) and (c) show nanodomains (2.5×2.5 μm scan).

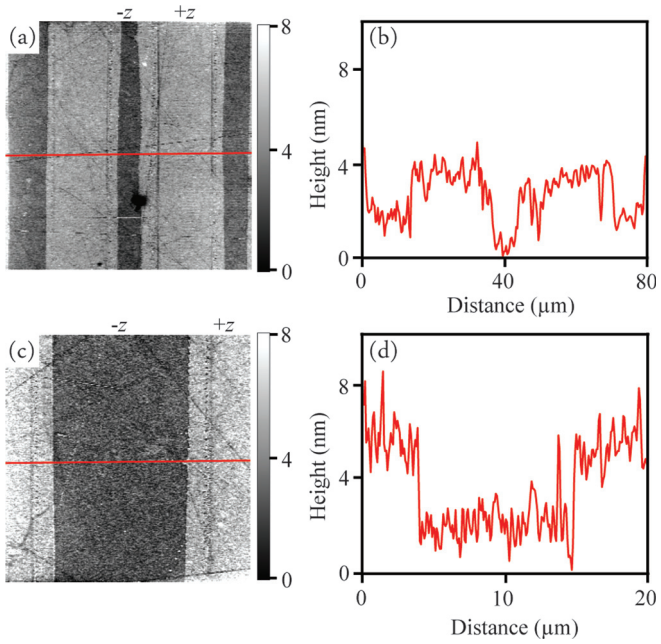

FIG. 3. (a) AFM topography image of an unannealed sample after photodeposition and (b) representative line profile. (c) Higher resolution AFM topography image of region shown in (a) and (d) representative line profile.

4.96 ± 0.95 nm. However, from the AFM images and line profile in Fig. 4, there appears to be an equal amount of Ag deposition on the positive and negative domains.

Photodeposition experiments repeated on the $+z$ 1D PPLN side provided complementary results; the positive domains were preferentially decorated with Ag in the unannealed sample, while the 180° domain walls were preferentially decorated in the annealed sample. Photodeposition experiments performed on both sides of unannealed and annealed 2D PPLN samples (Figs. 5(a)–5(d)) were

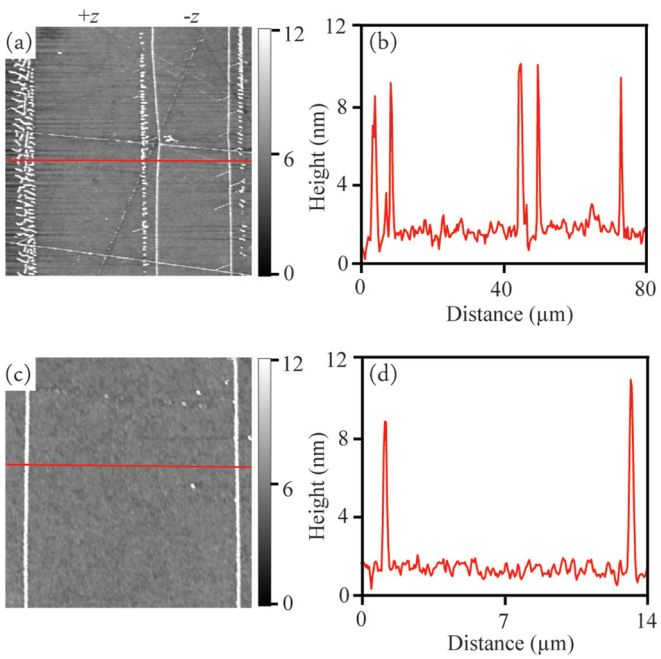

FIG. 4. (a) AFM topography image of an annealed sample after photodeposition and (b) representative line profile. (c) Higher resolution AFM topography image of region shown in (a) and (d) representative line profile.

qualitatively similar to the 1D case, highlighting that the Ag deposition does not depend on the domain shape or size. Furthermore, photodeposition experiments were conducted several times on both types of samples, leading to the same results, which corroborates the high reproducibility of these findings.

Whereas the PFM signal is expected to be proportional to the spontaneous polarization and in principle might be sensitive to the presence of defect dipoles, in practice, various sources of cross-talk can obfuscate small variations in PFM amplitude across a domain wall.[40] However, the Raman spectrum of PPLN is sensitive to electric fields and corresponding electromechanical strains in the crystal lattice. Most of the 4 A(LO) and 7 nonstoichiometric E(TO) peaks permitted in the chosen configuration[43] exhibit changes between poled and unpoled domain surfaces before annealing, which are not observed on the annealed sample.[44] A(LO) characterizes longitudinal ion oscillation along the z-axis whereas E(TO) represents transversal motion in x- or y-direction. In Figs. 5(e) and 5(f), maps of the peak intensity, position, and width for the $A(LO_3)$ and $E(TO_4)$ bands at around 424 and 431 cm^{-1}, respectively, are depicted. The intensity and FWHM of the $A(LO_3)$ band of unannealed PPLN show clear contrast between domain surfaces, whereas a peak position shift is observed at domain walls. Upon annealing, only a weak contrast at domain walls persists for all peak parameters. The intensity, position, and FWHM of the $E(TO_4)$ band exhibits differences between poled and unpoled domains before annealing, and it is observed only at domain walls on the annealed substrate. Apart from the A(LO) and E(TO) modes, a weak peak around 615 cm^{-1}, which according to previous reports, originates from forbidden $A(TO_4)$ oscillations due to symmetry breaking, was also detected.[45,46] This band originates from Nb octahedron related structural damage, which is most pronounced at domain walls on both samples (Fig. 5(g)). The peak around 732 cm^{-1} is ascribed to defects representing ilmenite-like stacking faults that originate from the presence of Nb_{Li} and involve a change in the cation sequence.[46,47] Similar to the $E(TO_7)$ band, this defect peak shows contrast between domains on the unannealed sample but only varies at domain walls on the annealed sample (Fig. 5(h)).

IV. DISCUSSION

Here, a model (Fig. 6) is proposed based on (a) what occurs to the LN crystal during poling, (b) how poling affects photodeposition on PPLN, (c) what occurs to the PPLN crystal during annealing, and (d) how annealing affects photodeposition on PPLN.

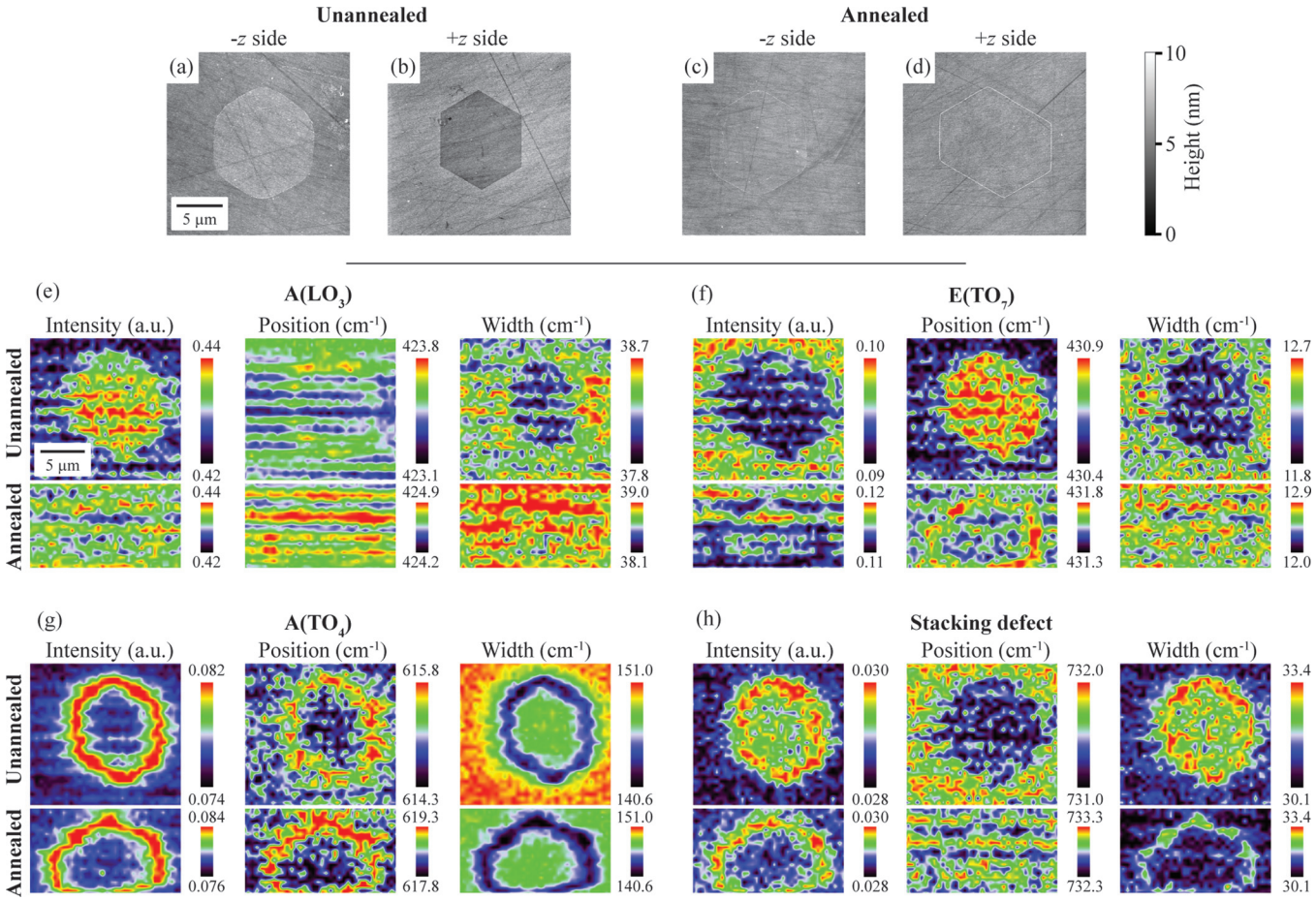

FIG. 5. AFM topography images after photodeposition on 2D PPLN (a,b) unannealed and (c,d) annealed samples ((a) and (c) initial $-z$ side, (b) and (d) initial $+z$ side). Corresponding Raman maps measured on $+z$ sides before and after annealing showing peak parameter (intensity (a.u.), position (cm^{-1}), and width (cm^{-1}) according to map labels) for (c) $A(LO_3)$, (f) $E(TO_7)$, (g) $A(TO_4)$, and (h) a stacking defect band.

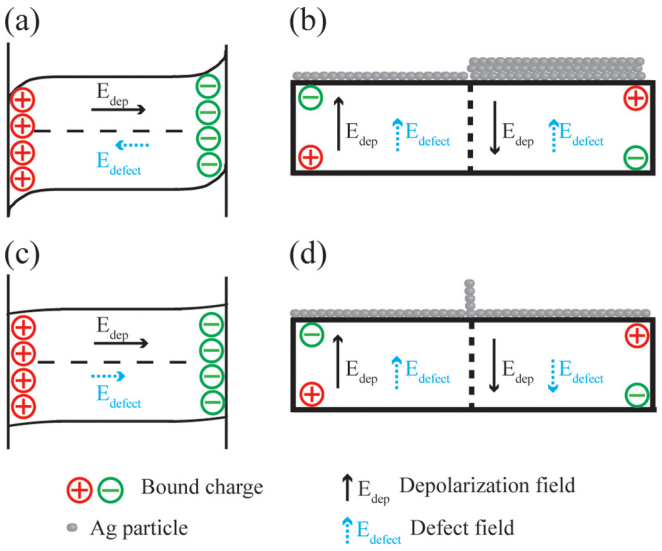

FIG. 6. Schematics showing electronic band diagrams for the $+z$ poled domain (a) before and (c) after annealing and the corresponding distribution of photodeposited Ag on PPLN (b) before and (d) after annealing (initial $-z$ side).

A. Influence of poling on the crystal structure of LN

When the polarization of LN is switched, the defect field in the poled domain is in a frustrated state, having an orientation antiparallel to the depolarization field since the V_{Li} cannot rearrange around the new Nb_{Li} position as a result of the low ion mobility of Li^+ at room temperature. The presence of this defect dipole can lead to increased band bending.[14] The resulting asymmetry in internal electric fields and corresponding electromechanical strains can be detected with Raman spectroscopy even a year after poling.

B. Photodeposition on unannealed PPLN

The regions where Ag deposits reflect where photogenerated electrons accumulate. Band bending and corresponding internal fields are known to influence electron accumulation.[13] After periodic poling and prior to annealing, Ag deposits on both negative and positive domain surfaces, however, there is preferential deposition on the positive surface (Fig. 3(a)), indicating more electrons accumulate at this surface in agreement with observations from literature, e.g., by Liu *et al.*[23] Downwards band bending pushes the photogenerated electrons towards the surface of the positive domain where they can reduce Ag^+ (Figs. 6(a) and 6(b)).[25] Conversely, the upwards band bending of the original negative domain is expected to push photogenerated electrons away from the surface towards the bulk. As a result, oxidation is typically reported to occur on negative domains on ferroelectric semiconductors,[3,8,48–51] whereby the spatial separation of oxidation and reduction reactions are reported to reduce recombination and back-reactions.[8,48] However, here, reduction is observed to occur to some extent on the negative domains. Deposition on negative domains has been previously attributed to the photoelectric effect, whereby the energy of the incident light, in conjunction with the weak band bending of LN compared to other ferroelectric materials,[14,26] is sufficient for some electrons to leave the surface and participate in the reduction reaction.[24,52]

The Raman maps shown in Figs. 5(e), 5(f), and 5(h) corroborate the presence and influence of the defect frustration in the poled regions and show a strong correlation with the photodeposition maps (Figs. 1(a), 5(a), and 5(b)), wherein Ag deposition is pronounced for the positive domain surfaces.

C. Influence of annealing on the crystal structure of PPLN

Upon annealing, the ion mobility of Li^+ increases at temperatures $>150\,^{\circ}C$. The movement of Li^+ ions leads to the reorientation of the defect cluster and corresponding realignment of the defect field parallel to the depolarization field. This realignment results in the removal of the poling induced asymmetries between the domains (shown in Fig. 6(d)) compared to the unannealed case (Fig. 6(a)) for positive and negative domains. As the presence of photodeposited Ag indicates where electrons accumulate, it is proposed that annealing leads to reorientation of defect dipoles, reduced band bending (Fig. 6(c)), and a higher probability of electron-hole recombination.[14,48] Correspondingly, the contrast in Raman maps between domain surfaces disappears upon annealing (Figs. 5(e), 5(f), and 5(h)). However, pronounced contrast at domain walls, especially in Fig. 5(g), suggests the presence of strain and related structural distortions at these interfaces.

D. Photodeposition on annealed PPLN

On annealed PPLN, while the positive and negative domains had a similar amount of Ag, there was more Ag on the 180° domain wall (Fig. 6(c)), as has been reported in the previous studies.[14,15,25,26] The deposition on the negative surface was similar to the deposition achieved before annealing. Furthermore, the similar level of deposition on positive and negative domains suggests a similar electron flux at both surfaces and/or a similar photodeposition mechanism. Annealing removed the asymmetry in the internal fields, likely reducing the band bending at the $+z$ poled surface and increasing the likelihood of recombination over reduction.[14] Further work is needed to elucidate the exact role of photoelectric and photovoltaic electrons, including those from trapped states, on photodeposition.

The enhanced deposition of Ag along the domain wall has been previously reported by Hanson *et al.* on congruent PPLN samples from Crystal Technology (and also on stoichiometric PPLN) to result from the presence of defects and the in-plane electric field at the domain wall.[14] A similar situation is expected in the annealed samples discussed here; the defect dipoles reorient, reducing band bending after annealing.[14] These factors act cooperatively to reduce the accumulation of electrons and hence the amount of Ag deposition on the positive surface, increase the likelihood of electron-hole recombination, and allow the electron accumulation to be guided by the in-plane electric field and the presence of structural distortions at the domain wall. Both the realignment of the defect field with depolarization in the positive poled domain and the presence of structural distortions located at the domain wall have been corroborated by Raman spectroscopy (Figs. 5(e)–5(h)). On Gooch &

Housego and Crystal Technology PPLN samples, deposition (not shown) was found to be similar to the annealed sample studied here and took place preferentially on the domain walls in the absence of annealing, further highlighting the importance of understanding the influence of defect density and thermal treatment on photodeposition.

V. CONCLUSIONS

It is demonstrated here that Ag photodeposition occurs preferentially on the positive domains of unannealed PPLN crystals as a result of downwards band bending. Upon annealing, the Ag deposition is approximately equivalent on positive and negative domain surfaces while at 180° domain walls the deposition is more pronounced. It is proposed that annealing mobilized Li^+ ions and realigned the defect field in the same direction as the depolarization field, as confirmed using Raman spectroscopy. The realignment promoted the preferential deposition of Ag along domain walls characterized by defects and the presence of an in plane field, which acts to prevent electron-hole recombination, was promoted. By elucidating the role of thermal treatments on the photochemistry of ferroelectric crystals, further guidance on the optimization of the fabrication of metallic nanostructure arrays on ferroelectric templates for biosensing applications is provided.

ACKNOWLEDGMENTS

This publication has emanated from research conducted with the financial support of the DGPP and NANOREMEDIES, which are funded under the Programme for Research in Third Level Institutions (PRTLI) Cycle 5 and co-funded by the European Regional Development Fund. This research was also funded by the European Commission within FP7 Marie Curie Initial Training Network "Nanomotion" (Grant Agreement No. 290158), the Swedish Scientific Research Council (VR 622-2010-526 and 621-2011-4040), and the ADOPT Linnaeus Centre for Advanced Optics and Photonics in Stockholm. Raman measurements were conducted at the Center for Nanophase Materials Sciences which is a DOE Office of Science User Facility (CNMS2015-139). The AFM used for this work was funded by Science Foundation Ireland (SFI07/IN1/B931). The authors gratefully acknowledge D. Denning for assistance with PFM analysis.

[1]X. Liu, K. Kitamura, Q. Yu, J. Xu, M. Osada, N. Takahiro, J. Li, and G. Cao, Sci. Technol. Adv. Mater. **14**, 055011 (2013).
[2]S. Damm, N. C. Carville, B. J. Rodriguez, M. Manzo, K. Gallo, and J. H. Rice, J. Phys. Chem. C **116**, 26543 (2012).
[3]S. Kalinin, D. Bonnell, T. Alvarez, and X. Lei, Nano Lett. **2**, 589 (2002).
[4]M. Hnilova, X. Liu, E. Yuca, C. Jia, B. Wilson, A. Y. Karatas, C. Gresswell, F. Ohuchi, K. Kitamura, and C. Tamerler, ACS Appl. Mater. Interfaces **4**, 1865 (2012).
[5]W.-C. Yang, B. J. Rodriguez, A. Gruverman, and R. J. Nemanich, Appl. Phys. Lett. **85**, 2316 (2004).
[6]D. Tiwari and S. Dunn, J. Mater. Sci. **44**, 5063 (2009).
[7]J. L. Giocondi and G. S. Rohrer, Chem. Mater. **13**, 241 (2001).
[8]J. L. Giocondi and G. S. Rohrer, J. Phys. Chem. B **105**, 8275 (2001).
[9]P. M. Jones and S. Dunn, Nanotechnology **18**, 185702 (2007).
[10]P. M. Jones, D. E. Gallardo, and S. Dunn, Chem. Mater. **20**, 5901 (2008).
[11]P. M. Jones and S. Dunn, J. Phys. D. Appl. Phys. **42**, 065408 (2009).
[12]S. Dunn, S. Sharp, and S. Burgess, Nanotechnology **20**, 115604 (2009).
[13]S. Dunn, P. M. Jones, and D. E. Gallardo, J. Am. Chem. Soc. **129**, 8724 (2007).
[14]J. N. Hanson, B. J. Rodriguez, R. J. Nemanich, and A. Gruverman, Nanotechnology **17**, 4946 (2006).
[15]A. Haussmann, P. Milde, C. Erler, and L. M. Eng, Nano Lett. **9**, 763 (2009).
[16]K. Seal, B. J. Rodriguez, I. N. Ivanov, and S. V. Kalinin, Adv. Opt. Mater. **2**, 292 (2014).
[17]N. C. Carville, M. Manzo, S. Damm, M. Castiella, L. Collins, D. Denning, S. A. L. Weber, K. Gallo, J. H. Rice, and B. J. Rodriguez, ACS Nano **6**, 7373 (2012).
[18]N. C. Carville, M. Manzo, D. Denning, K. Gallo, and B. J. Rodriguez, J. Appl. Phys. **113**, 187212 (2013).
[19]S. Damm, N. Craig Carville, M. Manzo, K. Gallo, S. G. Lopez, T. E. Keyes, R. J. Forster, B. J. Rodriguez, and J. H. Rice, Appl. Phys. Lett. **103**, 083105 (2013).
[20]L. Balobaid, N. C. Carville, M. Manzo, K. Gallo, and B. J. Rodriguez, Appl. Phys. Lett. **102**, 042908 (2013).
[21]L. Balobaid, N. Craig Carville, M. Manzo, L. Collins, K. Gallo, and B. J. Rodriguez, Appl. Phys. Lett. **103**, 182904 (2013).
[22]X. Y. Liu, F. Ohuchi, and K. Kitamura, Funct. Mater. Lett. **1**, 177 (2008).
[23]X. Y. Liu, K. Kitamura, K. Terabe, H. Hatano, and N. Ohashi, Appl. Phys. Lett. **91**, 044101 (2007).
[24]S. Dunn and D. Tiwari, Appl. Phys. Lett. **93**, 092905 (2008).
[25]Y. Sun, B. S. Eller, and R. J. Nemanich, J. Appl. Phys. **110**, 084303 (2011).
[26]Y. Sun and R. J. Nemanich, J. Appl. Phys. **109**, 104302 (2011).
[27]M. Yamada, N. Nada, M. Saitoh, and K. Watanabe, Appl. Phys. Lett. **62**, 435 (1993).
[28]Z. W. Hu, P. A. Thomas, and J. Webjorn, J. Phys. D. Appl. Phys. **28**, A189 (1995).
[29]D. Scrymgeour and V. Gopalan, Phys. Rev. B **72**, 024103 (2005).
[30]S. Kim, V. Gopalan, K. Kitamura, and Y. Furukawa, J. Appl. Phys. **90**, 2949 (2001).
[31]V. Gopalan, V. Dierolf, and D. A. Scrymgeour, Annu. Rev. Mater. Res. **37**, 449 (2007).
[32]V. Gopalan and M. C. Gupta, Ferroelectrics **198**, 49 (1997).
[33]M. de Angelis, S. De Nicola, A. Finizio, G. Pierattini, P. Ferraro, S. Grilli, and M. Paturzo, Appl. Phys. Lett. **85**, 2785 (2004).
[34]G. Bhagavannarayana, G. C. Budakoti, K. K. Maurya, and B. Kumar, J. Cryst. Growth **282**, 394 (2005).
[35]V. Gopalan and M. C. Gupta, Appl. Phys. Lett. **68**, 888 (1996).
[36]V. Gopalan, T. E. Mitchell, Y. Furukawa, and K. Kitamura, Appl. Phys. Lett. **72**, 1981 (1998).
[37]M. Manzo, F. Laurell, V. Pasiskevicius, and K. Gallo, Opt. Mater. Express **1**, 365 (2011).
[38]A. M. Prokhorov and I. U. S. Kuzminov, *Physics and Chemistry of Crystalline Lithium Niobate* (Hilger, Bristol/New York, 1990).
[39]B. J. Rodriguez, R. J. Nemanich, A. Kingon, A. Gruverman, S. V. Kalinin, K. Terabe, X. Y. Liu, and K. Kitamura, Appl. Phys. Lett. **86**, 012906 (2005).
[40]D. Denning, J. Guyonnet, and B. J. Rodriguez, Int. Mater. Rev. (to be published).
[41]V. Y. Shur, *Correlated Nucleation and Self-Organized Kinetics of Ferroelectric Domains* (Wiley-VCH Verlag GmbH & Co. KGaA, 2005).
[42]V. Y. Shur, E. Rumyantsev, E. Nikolaeva, E. Shishkin, R. G. Batchko, G. D. Miller, M. M. Fejer, and R. L. Byer, Proc. SPIE **7**, 143 (2000).
[43]J. G. Scott, S. Mailis, C. L. Sones, and R. W. Eason, Appl. Phys. A Mater. Sci. Process. **79**, 691 (2004).
[44]S. M. Neumayer, *Interface Modulated Charge Transport and Ferroelectric Switching in Lithium Niobate* (University College Dublin, 2015).
[45]G. R. Paz-Pujalt and D. D. Tuschel, Appl. Phys. Lett. **62**, 3411 (1993).
[46]H.-C. Huang, J. I. Dadap, O. Gaathon, I. P. Herman, R. M. Osgood, S. Bakhru, and H. Bakhru, Opt. Mater. Express **3**, 126 (2013).
[47]Y. Kong, J. Xu, X. Chen, C. Zhang, W. Zhang, and G. Zhang, J. Appl. Phys. **87**, 4410–4414 (2000).
[48]L. Li, P. A. Salvador, and G. S. Rohrer, Nanoscale **6**, 24 (2014).
[49]S. V. Kalinin, D. A. Bonnell, T. Alvarez, X. Lei, Z. Hu, R. Shao, and J. H. Ferris, Adv. Mater. **16**, 795 (2004).
[50]M. Stock and S. Dunn, J. Phys. Chem. C **116**, 20854 (2012).
[51]X. Lei, D. Li, R. Shao, and D. A. Bonnell, J. Mater. Res. **20**, 712 (2005).
[52]W.-C. Yang, B. J. Rodriguez, A. Gruverman, and R. J. Nemanich, J. Phys. Condens. Matter **17**, S1415 (2005).